Automatic Channel Network Extraction From Remotely Sensed Images by Singularity Analysis

Furkan Isikdogan, Alan Bovik, and Paola Passalacqua

Abstract—The quantitative analysis of channel networks plays an important role in river studies. To provide a quantitative representation of channel networks, we propose a new method that extracts channels from remotely sensed images and estimates their widths. Our fully automated method is based on a recently proposed multiscale singularity index that strongly responds to curvilinear structures but weakly responds to edges. The algorithm produces a channel map using a single image where water and nonwater pixels have contrast, such as a Landsat near-infrared band image or a water index defined on multiple bands. The proposed method provides a robust alternative to the procedures that are used in the remote sensing of fluvial geomorphology and makes the classification and analysis of channel networks easier. The source code of the algorithm is available at http://live.ece.utexas.edu/research/cne/.

Index Terms—Channel network extraction, deltas, image processing, remote sensing, river width.

I. INTRODUCTION

A METHOD for the completely automatic extraction of channel networks from satellite imagery could greatly facilitate the monitoring of water resources by eliminating the laborious process of manual inspection. Such a method could be used for creating quantitative representations of channel networks, which would be useful in a wide variety of studies. The automatic extraction of channel networks is particularly challenging in coastal areas due to low topographic gradients, the presence of features such as sediment plumes, and the wide range of scales over which channel features are present. A robust channel extraction method would ease monitoring coastal areas and analyzing deltaic response to anthropogenic forcing and natural forcing over large spatial areas and long temporal intervals.

Several approaches have been suggested to extract curvilinear structures from remotely sensed images, with many of them focusing on road network extraction [1]–[6]. Based on the road network extraction in [2] and [3], a method has been proposed to detect rivers as linear structures, imposing constraints on the river length, the curvature, and the confluences

for connectivity [7]. A software tool, i.e., *RivWidth* [8], has been proposed for calculating river centerlines and widths. RivWidth (v0.4) requires the availability of a previously defined binary mask that indicates water and nonwater pixels. Although such a mask could be extracted from remotely sensed images by thresholding and using shape-correcting operations, the manual cleaning of the mask would be often necessary to separate the true water mask from spurious responses [9]. Our new method can estimate the channel centerline, width, and orientation, and it can create a map of a channel network in a purely automatic manner only using remotely sensed data. To the best of our knowledge, this is the first fully automatic approach that provides these outputs.

II. MODIFIED MULTISCALE SINGULARITY INDEX

The multiscale singularity index [10], [11] is a useful method for detecting singular curvilinear structures over multiple scales. The algorithm is useful for locating channels in satellite images. However, the presence of channels over a wide range of scales creates some artifacts in the singularity index response. Our work modifies and extends the multiscale singularity index to address the multiscale nature of channel networks. The multiscale singularity index algorithm and our modifications are briefly explained in the following sections.

A. Multiscale Singularity Index

At each pixel, the multiscale singularity index algorithm first estimates direction θ orthogonal to the curvilinear mass using the second-order derivatives of an input image along evenly spaced directions. Then, it computes the singularity index at each scale as

$$(\psi f)(x,y,\sigma) = \frac{|f_{0,\theta,\sigma}(x,y) f_{2,\theta,\sigma}(x,y)|}{1 + |f_{1,\theta,a\sigma}(x,y)|} \tag{1}$$

where $f_{0,\theta,\sigma}(x,y)$, $f_{1,\theta,\sigma}(x,y)$, and $f_{2,\theta,\sigma}(x,y)$ are the zero-, first-, and second-order Gaussian derivatives at scale σ and along direction $\theta(x,y)$. In the denominator, a is a constant with a recommended value of 1.7754. This value results in the maximum attenuation of the sidelobe response of the index [10]. Index $(\psi f)(x,y,\sigma)$ is computed over N scales $\sigma_n = \sigma_1 \sqrt{2}^{(n-1)}$ for $n = 1, 2, \ldots, N$. The window sizes for the image filters are determined to be $\lceil 6\sigma \rceil$. Since a channel with a width larger than the image dimensions cannot be detected by the algorithm, an upper bound for the number of scales N can be determined by having the filter dimensions smaller
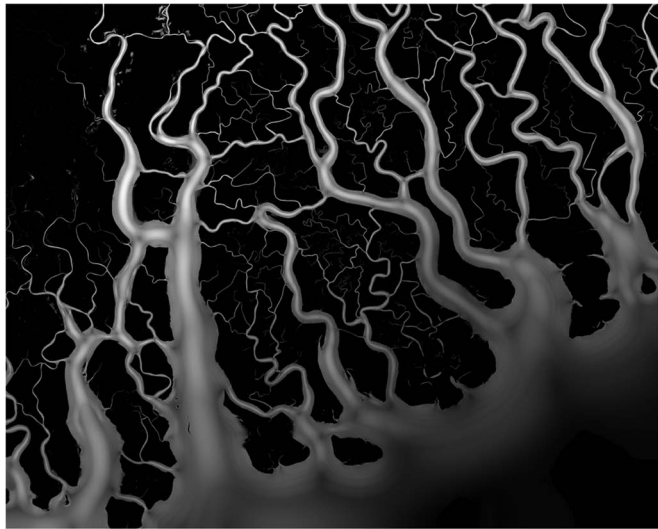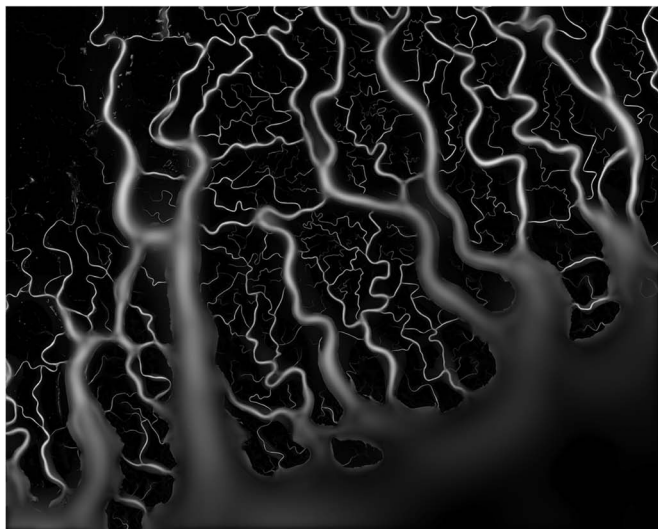
(a)

(b)
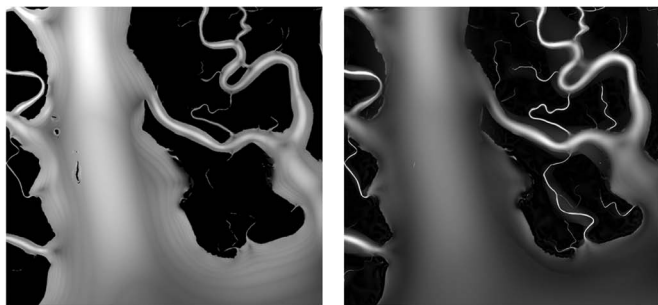
(c)   (d)

Fig. 1. Comparison of the original and modified multiscale singularity index responses. Full-sized images: (a) original response and (b) modified response. Zoomed images: (c) original response and (d) modified response.

than image dimensions $M \times M$ so that $6\sigma_1\sqrt{2}^{(N-1)} \leq M$ as follows:

$$N = \left\lceil \frac{2\log\frac{M}{6\sigma_1}}{\log 2} + 1 \right\rceil . \tag{2}$$

After computing the singularity index at each scale, the algorithm finds the maximum response across all scales at each pixel location.

Fig. 2. Typical results of centerline extraction.

The singularity index retains the polarity, which is useful for discriminating between the channel and island responses since channels and islands have opposite polarities. By discarding the negative polarity, we remove the island response.

B. Debiasing Input Images

An input image should be debiased before computing the singularity index in order to achieve invariance to the local direct-current offset. The multiscale singularity index algorithm debiases an input image by subtracting a large Gaussian filter from the original image, which essentially performs local mean subtraction. This approach works well for a small range of scales. For a large range of scales, however, a large Gaussian filter fails to debias finer scales and results in a loss of detail at fine scales [see Fig. 1(a)]. To address this problem, we debias the input image at every scale. Instead of using one large Gaussian filter over all scales, our modified version of the multiscale singularity index uses a Gaussian filter with a standard deviation of σ_n at each scale as

$$I_\sigma = I - \mathcal{G}_\sigma * I \tag{3}$$

where I_σ is the debiased image at scale σ, I is the input image, and $\mathcal{G}_\sigma$ is the Gaussian filter.

C. Width Estimation

The channel width is estimated by interpolating between the scale that has the highest singularity index response ψ and its neighbor scales as follows:

$$w(x,y) = k\frac{\sum\limits_{i=-1}^{+1}\sigma_{m+i}(\psi f)(x,y,\sigma_{m+i})}{\sum\limits_{i=-1}^{+1}(\psi f)(x,y,\sigma_{m+i})} \tag{4}$$

where $m = \arg\max_n(\psi f)(x,y,\sigma_n)$ at spatial coordinate x,y, and k is a scalar variable that scales the output.
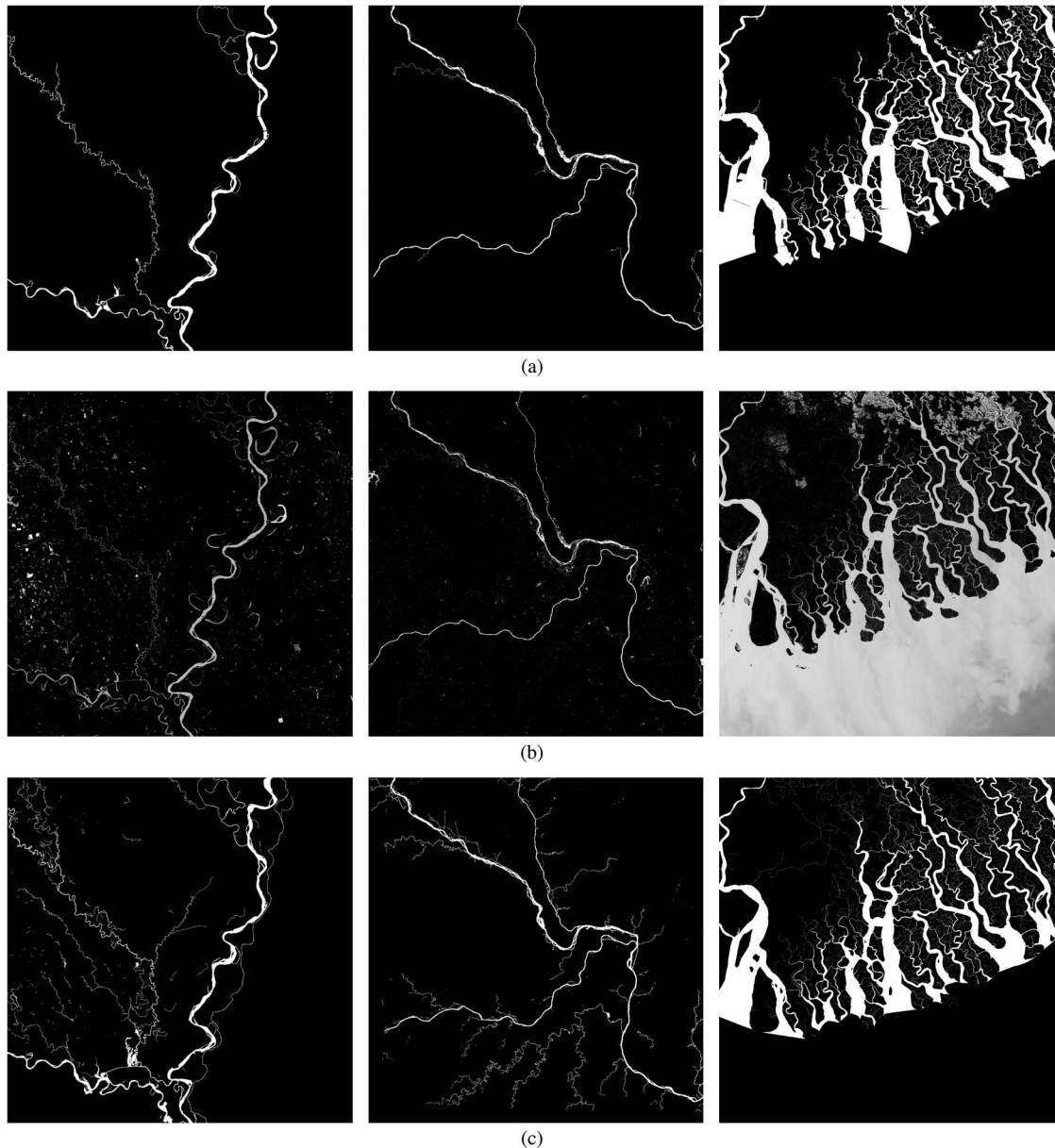
Fig. 3. Comparison of the (a) regrown channel maps with the (b) input and (c) ground-truth images. First column: Mississippi River near Memphis, TN. Second column: Mississippi, Missouri, and Illinois Rivers near St. Louis, MO. Third column: a portion of the GBJ Delta. Landsat IDs of the scenes: LC80230362015045LGN00, LC80240332014305LGN00, and LC81380452014304LGN00, respectively.

D. Adaptive Smoothing

The multiscale singularity index creates ripples near the banks of wide rivers when a large range of scales is processed [see Fig. 1(c)]. The ripples occur after finding the maximum response over all the scales at each spatial coordinate. To attenuate the ripples, we employ an adaptive smoothing algorithm that adjusts the strength of smoothing based on the estimated scale for each pixel so that coarse scales can be smoothed more than fine scales. To implement the adaptive smoothing algorithm in a computationally efficient way, we first compute an integral image over the singularity index response, which enables the fast computation of summations over regions of an arbitrary size. Then, we smooth the response using a box filter with a variable window size that is determined by the estimated scale. Since the integral image is only computed

once, the algorithm only needs to perform two additions and one subtraction per pixel. We iteratively apply the adaptive box filter to approximate a Gaussian filter.

The typical results delivered by the multiscale singularity index and by our modified version are compared in Fig. 1.

E. Centerline Extraction

To determine the channel centerlines, the maximum response across all the scales is computed at each coordinate, and the orientation value at the maximum-response scale is taken to be the dominant centerline direction. A process of nonmaxima suppression is applied along the dominant direction, as explained in [10]. Then, a threshold level T is determined on the nonmaxima suppressed (NMS) image using Otsu's method

[12]. To preserve the channel connectivity, a hysteresis threshold is applied to binarize the NMS image as follows.

1) Set the pixels above an error threshold ϵ to one and the rest to zero.
2) Find the connected components in the image.
3) Find and remove the connected components that do not have at least one pixel above threshold T.

Error threshold ϵ is empirically chosen as $0.1 \times T$. The extracted centerlines for an example input image are illustrated in Fig. 2. This figure is inverted for better visualization.

F. Creating Map of Channels

To show the computed channel width at each spatial co-ordinate along a centerline, a map of channels is created by regrowing the channels. The channels are regrown by drawing a line of length $w(x, y)$ and orientation $\theta(x, y)$ at each spatial location (x, y). The algorithm estimates the width of any water body with a width smaller than the largest scale. Therefore, the resultant map includes ponds and other small water bodies, as well as channels. The results of the channel map creation are presented in Section III.

III. EXPERIMENTS AND RESULTS

We tested our model on three different regions having different characteristics: the Mississippi River near Memphis, TN (I1); the Mississippi, Missouri, and Illinois Rivers near St. Louis, MO (I2); and a portion of the Ganges–Brahmaputra–Jamuna (GBJ) Delta (I3). We used Landsat-8 images, which were downloaded at http://earthexplorer.usgs.gov/, to create the input images for our algorithm. The algorithm requires input images to have a contrast between water and nonwater pixels. An example input could be a near-infrared image or a water index that uses multiple bands. In our experiments, the input images were created using the modified normalized difference water index [13], which is an effective way to extract water information from remote sensing imagery.

The ground truth for I1 and I2 are obtained by aligning, cropping, and rasterizing the river data from the National Hydrography Dataset (http://nhd.usgs.gov/). For I3, the GBJ Delta network extracted by the work in [9] is used as the ground truth. The extraction performed by the work in [9] included manual cleaning and a comparison with Google Earth imagery. Both the ground truth and the input images have rivers close to the mean discharge, making the results of our algorithm comparable with the ground truth.

We fixed the minimum scale σ_1 to its default value [10], i.e., 1.5 pixels, which is the smallest width for a channel to be captured by the algorithm. The number of scales is automatically determined using the upper bound that is described earlier. To reduce the computation time, a smaller number of scales could be also chosen if all channels of interest are known to be smaller than a certain width. In the experiments reported here, we set the number of scales N to 16.

The regrown channel maps, showing the estimated location, width, and orientation of the channels, are compared with the ground truth and input images in Fig. 3. The ground-truth images did not include nonchannel water bodies. Therefore, we

also removed the nonchannel water bodies from the regrown channel maps by discarding the connected components that constitute less than 0.1% of the maps. Given the ground-truth images, the accuracy values $((TP + TN)/(TP + TN + FP + FN))$ of the regrown channel network images were found to be 96.77%, 97.86%, and 91.13% for I1, I2, and I3, respectively.

IV. CONCLUSION AND FUTURE WORK

We have described an automatic channel network extraction algorithm that inputs remotely sensed images and produces maps of the estimated channel centerline, width, and orientation. We modified a multiscale singularity index to extract a network of channels over a wide range of scales. The algorithm automatically works without any user intervention.

Our method can be used to analyze channel networks in different environments and over time to capture the effect of environmental forcing and natural and anthropogenic changes on a network structure. One of our future research directions is to analyze the deltaic response to anthropogenic forcing and natural forcing in coastal areas. We also plan to extend our work toward automatically creating topological maps, which will provide the graph representations of channel networks.

REFERENCES

[1] A. K. Shackelford and C. H. Davis, "Fully automated road network extraction from high-resolution satellite multispectral imagery," in *Proc. IEEE IGARSS*, Jul. 2003, vol. 1, pp. 461– 463.

[2] F. Tupin, H. Maitre, J. F. Mangin, J. M. Nicolas, and E. Pechersky, "Detection of linear features in SAR images: Application to road network extraction," *IEEE Trans. Geosci. Remote Sens.*, vol. 36, no. 2, pp. 434– 453, Mar. 1998.

[3] M. Negri, P. Gamba, G. Lisini, and F. Tupin, "Junction-aware extraction and regularization of urban road networks in high-resolution SAR images," *IEEE Trans. Geosci. Remote Sens.*, vol. 44, no. 10, pp. 2962– 2971, Oct. 2006.

[4] C. Lacoste, X. Descombes, and J. Zerubia, "Point processes for unsupervised line network extraction in remote sensing," *IEEE Trans. Pattern Anal. Mach. Intell.*, vol. 27, no. 10, pp. 1568– 1579, Oct. 2005.

[5] C. Poullis and S. You, "Delineation and geometric modeling of road networks," *ISPRS J. Photogramm. Remote Sens.*, vol. 65, no. 2, pp. 165– 181, Mar. 2010.

[6] S. Valero, J. Chanussot, J. A. Benediktsson, H. Talbot, and B. Waske, "Advanced directional mathematical morphology for the detection of the road network in very high resolution remote sensing images," *Pattern Recognit. Lett.*, vol. 31, no. 10, pp. 1120– 1127, Jul. 2010.

[7] F. Cao, F. Tupin, J. Nicolas, R. Fjortoft, and N. Pourthie, "Extraction of water surfaces in simulated Ka-band SAR images of kaRIn on SWOT," in *Proc. IEEE IGARSS*, Jul. 2011, pp. 3562– 3565.

[8] T. Pavelsky and L. Smith, "RivWidth: A software tool for the calculation of river widths from remotely sensed imagery," *IEEE Geosci. Remote Sens. Lett.*, vol. 5, no. 1, pp. 70– 73, Jan. 2008.

[9] P. Passalacqua, S. Lanzoni, C. Paola, and A. Rinaldo, "Geomorphic signatures of deltaic processes and vegetation: The Ganges-Brahmaputra–Jamuna case study," *J. Geophys. Res., Earth Surf.*, vol. 118, no. 3, pp. 1838– 1849, Sep. 2013.

[10] G. S. Muralidhar, A. C. Bovik, and M. K. Markey, "A steerable, multiscale singularity index," *IEEE Signal Process. Lett.*, vol. 20, no. 1, pp. 7– 10, Jan. 2013.

[11] G. Muralidhar, A. Bovik, and M. Markey, "Noise analysis of a new singularity index," *IEEE Trans. Signal Process.*, vol. 61, no. 24, pp. 6150– 6163, Dec. 2013.

[12] N. Otsu, "A threshold selection method from gray-level histograms," *Automatica*, vol. 11, no. 285– 296, pp. 23– 27, 1975.

[13] H. Xu, "Modification of Normalized Difference Water Index (NDWI) to enhance open water features in remotely sensed imagery," *Int. J. Remote Sens.*, vol. 27, no. 14, pp. 3025– 3033, 2006.